Monitoring fatigue crack growth using magnetic stray field measurements

Meijers, P. C.; Malschaert, D. H.; Veljkovic, M.

DOI
10.1088/1742-6596/2647/18/182018

Publication date
2024

Document Version
Final published version

Published in
Journal of Physics: Conference Series

Journal of Physics: Conference Series

PAPER • **OPEN ACCESS**

Monitoring fatigue crack growth using magnetic stray field measurements

To cite this article: P C Meijers *et al* 2024 *J. Phys.: Conf. Ser.* **2647** 182018

Journal of Physics: Conference Series **2647** (2024) 182018 doi:10.1088/1742-6596/2647/18/182018

Monitoring fatigue crack growth using magnetic stray field measurements

P C Meijers, D H Malschaert and M Veljkovic

Department of Engineering Structures, Faculty of Civil Engineering and Geosciences, Delft University of Technology, Stevinweg 1, 2628 CN Delft, the Netherlands

E-mail: p.c.meijers@tudelft.nl

Abstract. To monitor the growth of fatigue cracks in steel specimens, several methods exists. In this paper, the magnetic stray field, which is generated by the magnetisation of the specimen, was measured during loading to investigate how to utilise this data to reliably monitor fatigue crack initiation and growth. Data was collected in a series of fatigue tests on Compact Tension specimens with different force ratios. The evolution of the mean value of the dominant stray field component displayed a sensitivity to stress, plastic deformation and displacement of the specimen. By analysing the stress field induced by the loading, these three causes were distinguished from another. Crack initiation was marked by a large change of the mean magnetic stray field. Moreover, the amplitude of the magnetic stray field components showed a clear peak, at which moment 20% of the life time of the specimen is remaining, indicating that the magnetic stray field might provide a useful method to monitor the evolution of fatigue cracks.

1. Introduction

Fatigue resistance of steel components is of major importance for the safety of infrastructures. Early detection of fatigue cracks in such structures means that appropriate repairs can be performed before the damage becomes too severe. Despite the need for a reliable early detection method for this type of damage, detection is notoriously difficult. Therefore, there is a need for innovative detection methods to improve or complement the current monitoring systems.

In the search for a new method to monitor the growth of fatigue cracks, the magnetic stray field generated by the magnetisation of the steel component becomes interesting, because the strength and direction of the magnetic stray field are strain-dependent. Several methods to detect and quantify fatigue crack growth have been investigated over the years. A first class of methods involves the generation of a relatively strong magnetic field in the vicinity of the specimen to magnetise the material during testing [1, 2]. From a practical perspective, these active magnetic methods are less attractive, as the constant generation of these magnetic field is unfeasible in terms of power consumption and required equipment. As a result, passive magnetic methods have received more interest recently. In these methods, no effort is made to control the external field, i.e. only the geomagnetic field is present.

A frequently-used passive monitoring technique is the Metal Magnetic Memory (MMM) method, in which the magnetic field of the specimen is registered along several scanning lines close to the crack tip while the specimen is unloaded [3]. The evolution of the magnetic stray field along the measurement line is then related to the crack growth [4]. However, for in-situ

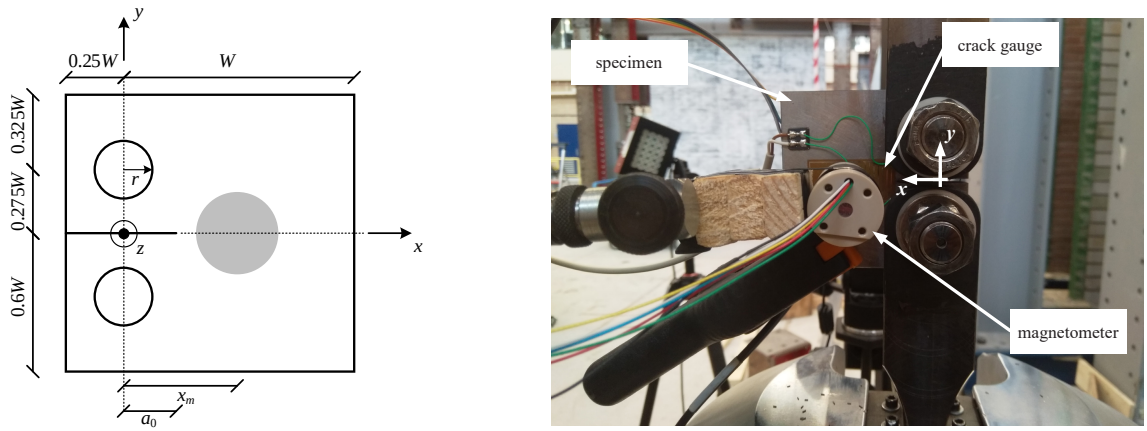

(a) (b)

Figure 1: (a) Dimensions of the CT specimens as a function of the specimen width W. (b) Annotated photograph of the back side of a specimen showing the magnetic field sensor and the crack gauge.

testing, it is impossible to stop the loading. Hence, some research has been done using time signals of the magnetic stray field [5, 6].

In this research, a similar approach has been taken, i.e. nine Compact Tension (CT) specimens have been subjected to cyclic loading until failure. The crack growth was monitored using two non-destructive techniques: a conventional crack gauge, and a magnetometer to measure the changes in the magnetic stray field in real-time. After that, the magnetomechanical characteristics have been defined and analysed to demonstrate how the magnetic stray field can be used to monitor crack initiation and growth in a ferromagnetic specimen.

2. Experimental set-up

In the following, the properties of the specimens and the sensors will be introduced. Then, the measurement procedure and the data processing is discussed.

2.1. Description of the specimens

During the experiment, nine identical CT specimens are cyclically loaded in tension until failure. The CT specimens are designed according to the ASTM standard [7], of which Figure 1a shows a schematic. In the figure, the following dimensions are indicated: specimen width $W = 70\,\text{mm}$, initial crack length $a_0 = 16\,\text{mm}$, and pin hole radius $r = 0.125W$. Each specimen is made of S355 structural steel and has a thickness of 14.1 mm. Note that the initial crack is present through the full thickness of the specimen. In Figure 1a, the gray circle denotes the magnetometer at the correct size. A photograph from the back side of the specimen and magnetometer is presented in Figure 1b. In relation of the initial magnetic properties, the specimens are not demagnetised prior to loading. This choice was made to create a scenario for the magnetic field that is realistic in practice, where demagnetising a structure prior to loading is not convenient.

The cyclic loading is generated by a test machine by applying a cyclic tensile force at the pin through the lower hole of the specimen, while the upper pin remains fixed. For all specimens, the force range is constant, i.e. $\Delta F = F_{\max} - F_{\min} = 15\,\text{kN}$, while the force ratio $R = F_{\min}/F_{\max}$ varies per specimen. In total, nine specimens are tested with three different loading ratios R, of which Table 1 gives an overview. During all tests, the loading frequency is kept constant at

Table 1: Overview of the tested specimens, indicating the minimum and maximum force, the resulting force ratio R, the distance between the magnetometer and the surface of the specimen d, the location of the magnetometer along the centre line x_m, and the employed crack gauge (CG).

Specimen	$F_{\min}$ [kN]	$F_{\max}$ [kN]	R [-]	d [mm]	x_m [mm]	CG
A1	5	20	0.25	20.5	38.6	MM
A2	5	20	0.25	29.5	39.5	MM
A3	5	20	0.25	-	-	MM
B1	15	30	0.50	23.1	20.1	A
B2	15	30	0.50	19.2	24.1	A
B3	15	30	0.50	-	-	A
C1	1.7	16.7	0.10	21.2	27.2	A
C2	1.7	16.7	0.10	21.0	28.9	A
C3	1.7	16.7	0.10	-	-	A

$f = 10\,\text{Hz}$.

2.2. Description of the sensors

To monitor the growth of the fatigue crack, crack gauges are employed at the tip of the initial crack. For specimens A1, A2 and A3, a *Micro Measurements* (MM) TK-09-CPC03-003 was used, which has a range of $\Delta a = 40\,\text{mm}$ and a relatively coarse grid interval of 2 mm. The other specimens were monitored using an *Althen* (A) FAC-20, which has a range of $\Delta a = 20\,\text{mm}$ and a grid interval of 0.5 mm.

The magnetic stray field generated by the specimen is measured by a tri-axial fluxgate magnetometer (*Stefan Mayer Instruments* FLC3-70), which has a measuring range of $\pm 200\ \mu\text{T}$, and a sensitivity of $0.035\ \mu\text{T/mV}$. For each specimen, the magnetometer is located at the centre line of specimen, i.e. the line $y = 0$. The position of the centre of the magnetometer along the x-axis is indicated by x_m, and the distance of the sensor with respect to the steel surface (i.e. the sensor's lift-off) is denoted by d. Table 1 lists these parameter for each of the specimens. Note that not all specimens have been probed using the magnetometer, only two specimens per R were equipped. When the magnetometer was not used, no value for d and x_m is given in Table 1.

2.3. Measurement procedure and data processing

During loading, times traces of the quantities of interest were not constantly recorded. After every 1000 loading cycles, data was logged during a period of 6 seconds, capturing approximately 60 loading cycles. The data was recorded with a sampling rate of 400 Hz to ensure that higher-order harmonics in the time signals can be captured with sufficient accuracy. These higher-order harmonics can result from non-linear interaction between the stress state and the magnetisation of the specimen.

As the prescribed loading is a purely harmonic signal, it is expected that the time signals of the other variables will also be harmonic. Therefore, it is convenient to define the following auxiliary variables to quantify the recorded time signals. For the generic variable q—which represents any time varying variable, e.g. the x-component of the magnetic field B_x—the mean of that variable will be denoted with an overline, i.e. $\overline{q}$, and it is defined as

$$\overline{q} = \frac{1}{N_s}\left(\sum_{i=1}^{N_s} q_i\right), \tag{1}$$

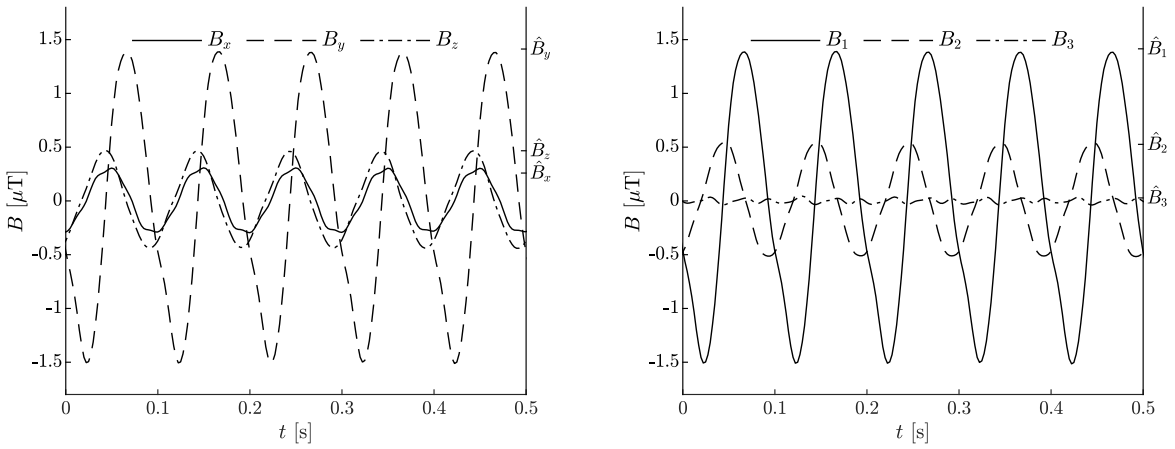

(a) (b)

Figure 2: Measured time trace of the magnetic field expressed in (a) the measured xyz-components and (b) the corresponding principle components.

in which q_i are the discrete realisations of the variable, and N_s is the number of sampling points. Second, to quantify the amplitude of a harmonic signal around the mean, the Root Mean Square (RMS) value of q is denoted by a hat, i.e. $\hat{q}$, and it is determined by

$$\hat{q} = \sqrt{2\,\overline{(q-\overline{q})^2}}, \tag{2}$$

in which the overlines denote the mean of the quantity below the line. In the above, the factor $\sqrt{2}$ is included to ensure the RMS value for a purely harmonic signal exactly equals the amplitude of that signal. The mean and RMS value of each quantity typify the full signal with only two scalar parameters.

The triaxial magnetometer registers the three components of the magnetic stray field, i.e. B_x, B_y and B_z, respectively. However, it is unlikely that the variability of the magnetic stray field is directed solely along one of these arbitrary directions. Hence, all magnetic field components should be analysed with respect to the stress field and the crack length. To simplify the analysis, the magnetic signal is projected onto its principle axes. Given the measured components, the principle components decomposition of the magnetic field $\mathbf{B}(t)$ is as follows [8]:

$$\mathbf{B}(t) = B_x(t)\,\mathbf{x} + B_y(t)\,\mathbf{y} + B_z(t)\,\mathbf{z} = B_1(t)\,\mathbf{e}_1 + B_2(t)\,\mathbf{e}_2 + B_3(t)\,\mathbf{e}_3, \tag{3}$$

in which $\mathbf{x}$, $\mathbf{y}$ and $\mathbf{z}$ represent the unit vectors in the measurement axes, and $\mathbf{e}_1$, $\mathbf{e}_2$ and $\mathbf{e}_3$ denote the unit vectors along the principle axes. In the above expression, $B_1(t)$, $B_2(t)$ and $B_3(t)$ denote the respective variations of the magnetic stray field along the principle axes.

To illustrate the decomposition, Figure 2a shows $\mathbf{B}(t)$ described in the measured xyz-components for five loading cycles. Note that the mean $\overline{\mathbf{B}}$ has been subtracted from the signal. It is clear that all three components of the magnetic field have a significant amplitude, which are labelled on the right axis of the figure. After applying the principle component decomposition, Figure 2a shows the time series of the computed components. It is easily verified that the maximum variability of the magnetic field is described by B_1, which is the essence of the principle component decomposition. Moreover, the amplitude of magnetic field along the third principle axis $\hat{B}_3$ is negligible compared to the other two components, effectively reducing the dimensionality of the vector field from three to two.

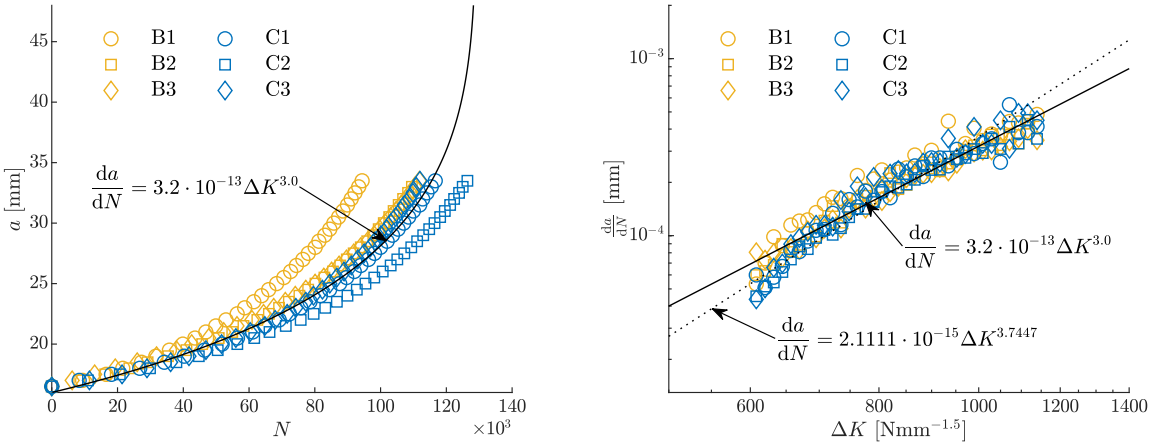

(a) (b)

Figure 3: (a) Crack growth against the number of cycles as measured by the crack gauges. (b) Crack growth rate against stress intensity factor range and two different linear fits.

3. Mechanical quantities

In this section, the mechanical quantities relevant for the magnetomechanical response will be discussed.

3.1. Crack growth

To assess the crack growth in the specimens, the data obtained from the crack gauges are analysed. Figure 3a presents the crack length a with increasing number of cycles N. Note that only the specimens with force ratios $R = 0.5$ and $R = 0.1$ are presented. The crack gauge used for the specimens with $R = 0.25$ had a too coarse grid to allow for a reliable fit of the data. Crack growth rates ($\frac{da}{dN}$) from the crack gauge measurements were determined following the procedures described in ASTM E647-15 [7]. These results are presented in a double logarithmic plot in Figure 3b. This presentation allows the data to be fit to Paris' relation:

$$\frac{da}{dN} = C\,(\Delta K)^m\,, \tag{4}$$

in which ΔK denotes the stress intensity factor range, and C and m are empirical constants, which can be determined from linear fitting with the experimental data. The stress intensity factor range is a function of the crack length, and it is determined using the expression provided by the ASTM standard [7]. In Figure 3b, two linear fits to the data are presented. The first fit has $C = 2.1111 \cdot 10^{-15}$ and $m = 3.7447$, resulting in a fit with $R^2 = 0.89$, in which the values for the empirical constants are taken from a study that tested CT specimens manufactured from the same steel grade [9]. The second trend line has $C = 3.2 \cdot 10^{-13}$ and $m = 3.0$, yielding $R^2 = 0.92$, and it represents the best fit to the crack growth data obtained in this study.

3.2. Stiffness

Next to the crack growth rate, the stiffness of the specimen is studied. From the amplitude of the applied force $\hat{F}$ and the amplitude of the resulting displacement $\hat{s}$, the stiffness of the specimen k is given by

$$k = \frac{\hat{F}}{\hat{s}}. \tag{5}$$

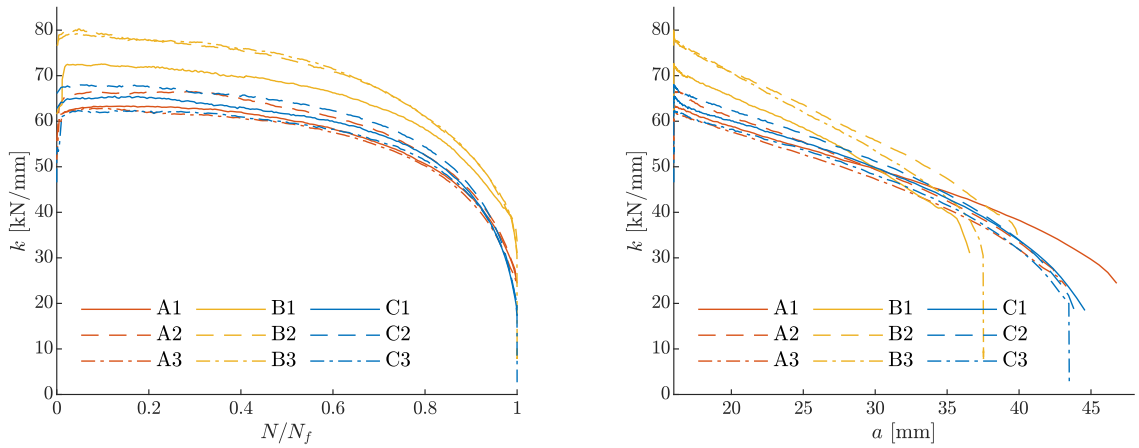

(a) (b)

Figure 4: Stiffness k of the specimens plotted against (a) the normalised number of cycles and (b) the crack length.

Figure 4a presents the stiffness with the number of cycles. It is clear that the stiffness remains relatively constant until failure is approached, when the stiffness decreases rapidly. A different perspective of the evolution of the stiffness is obtained by presenting the stiffness against crack length as in Figure 4b. This graph reveals that the stiffness is decreasing with increasing crack length in an approximately linearly fashion, which is a direct consequence of the changing geometry of the specimen. Since the force amplitude $\hat{F}$ is constant for all tests, the linear decrease of the stiffness implies that the amplitude of the displacement $\hat{s}$ increases linearly with the crack length.

3.3. Stress field

Since the magnetomechanical response is partially determined by the stress distribution in the specimen, the stress field generated by the tensile loading is computed by means of a linear elastic static simulation using the multiphysics Finite Element Analysis software *COMSOL* 5.6. For a static force $F = 15\,\text{kN}$, the Von Misses stresses for three different crack lengths are presented in Figure 5. These simulation results are only indicative for the true stress state, as the formation of plastic strain is not taken into account. Nonetheless, they give a valuable insight into the evolution of the stress distribution as the crack grows.

Initially ($a = a_0$), the highest stresses are concentrated in a small region around the crack tip (Figure 5a), and the main stress component is σ_{yy}. When the crack grows (Figure 5b), this region of highest stress moves with crack tip, and it increases in size. Conversely, just above and below the original position of the crack, i.e. around $x = a_0$, the stress levels have decreased significantly as result of the stress being forced to another path around the developed crack. At failure ($a = 3a_0$), the remaining cross section of the specimen experiences stress levels above the yield stress (Figure 5c), indicating that the specimen will plastically deform and fail.

4. Magnetic quantities

In this section, the evolution of two parameters of the magnetic field signals is presented with respect to the formation of the fatigue crack. First, the mean value of the magnetic field is discussed. Second, the amplitude of the time variation is analysed.

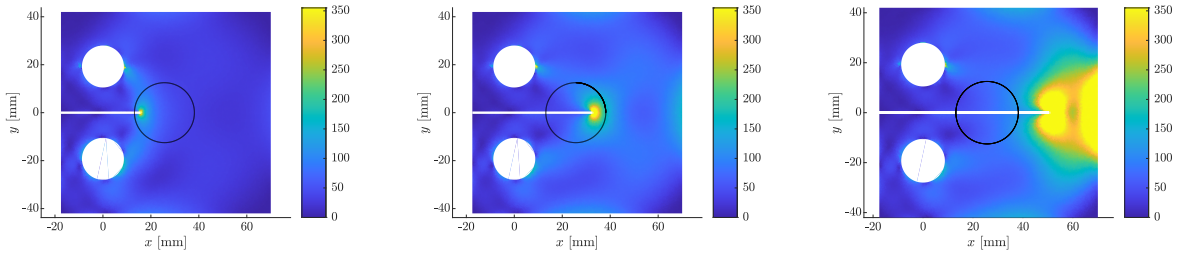

(a) $a = a_0$ (b) $a = 2a_0$ (c) $a = 3a_0$

Figure 5: Von Misses stresses [MPa] computed for $F = 15\,\mathrm{kN}$ with increasing crack length a. The black circle indicates the location of the magnetometer for specimen C1.

4.1. Mean of the magnetic signal

The magnetic stray field recorded by the magnetometer is directly proportional to the magnetisation of the specimen. Since the magnetisation is (not exclusively) influenced by the stress and the amount of plastic deformation, the mean magnetic stray field $\overline{\mathbf{B}}$ reflects the current and past stress state of the material. A change of the mean magnetic field $\overline{\mathbf{B}}$ with increasing crack length is measured in the following three situations [10]:

(i) when the magnetisation is not yet at a magnetic equilibrium, elastic deformation pushes the magnetisation towards this equilibrium, causing an increase of the magnetisation, and thus the measured magnetic field;

(ii) when a region of plastic deformation develops in the proximity of the magnetometer, which results in a decrease of the magnitude of the magnetisation;

(iii) when the specimen displaces with respect to the magnetometer, another distribution of magnetisation is registered by the sensor.

In these situations, the former two pertain to a direct change of the magnetisation due to (in)elastic strain, while the latter is caused by motion of the specimen as a whole. Separating these three causes might be difficult, as these can occur simultaneously. Fortunately, the simulated stress distribution as discussed in the previous section provides some guidance in that respect.

Of the three components of the mean magnetic stray field, only $\overline{B}_y$ changes significantly. By defining the change of the mean magnetic field as $\Delta\overline{B}_y = \overline{B}_y - \overline{B}_y^0$—the latter being the mean value during the first cycles—Figure 6a presents the evolution of the mean magnetic field with the number of cycles. Initially, the mean value remains constant, but it decreases exponentially when the number of cycles increases. The data for specimen B2 deviates from this general behaviour, which might be caused by the fact that the specimens are not demagnetised before the start of the test, giving each specimen an unknown initial magnetistion distribution.

More insightful is the change of the mean magnetic stray field with increasing crack length as presented in Figure 6b. During the initial growth of the crack, the stress in the vicinity of the magnetometer increases as the crack tip propagates in front of the sensor. This high stress leads to a substantial change of the magnetisation in that region, and thus of the measured mean stray field. Hence, crack initiation is clearly marked by a large change in the remanent magnetic stray field. Naturally, a criterion to definitively indicate a crack has initiated based on magnetic stray field measurement has to be defined. Further research into this phenomenon is required to define such a criterion.

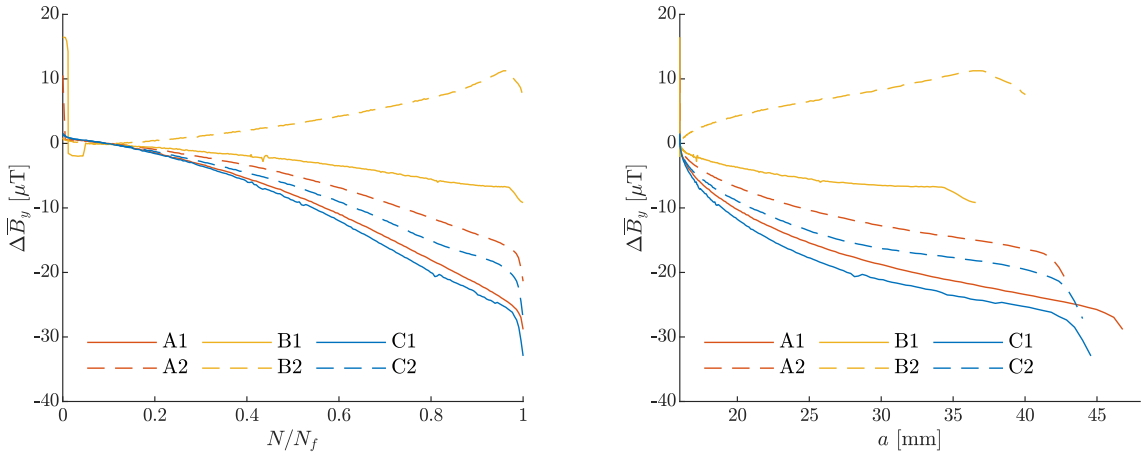

(a) (b)

Figure 6: Change of the mean value of the magnetic field component $\Delta\overline{B}_y$ against (a) the normalised number of cycles and (b) the crack length.

When the crack grows, and the crack tip has passed the magnetometer, the stress levels close to the magnetometer reduce significantly, and the variation of the magnetic field is only caused by the motion $\hat{s}$ of the specimen with respect to the sensor. As the displacement $\hat{s}$ increases linearly with the crack length, i.e. the process of crack opening, the mean stray field is also changing in a linear manner, which is clear in the graph for larger a. For specimens B1 and B2, which have a considerably higher $F_{\max}$ than the other specimens, a larger region of plastic deformation is formed around the crack. As plastic strain reduces the magnetic properties of the material [10], the remanent magnetic field is lower, resulting in a lower change of the mean magnetic field for these two specimens.

4.2. Amplitude of the magnetic signals

Figure 7 presents the amplitudes of the magnetic stray field, $\hat{B}_1$ and $\hat{B}_2$, with the number of cycles normalised by the cycle number at which the specimen failed, in which a clear pattern emerges: the amplitude of both components increases and has a maximum before failure. For each specimen, the maximum, which occurs at cycle $N_{\hat{B}_1}$ and $N_{\hat{B}_2}$, is indicated in the graphs by a circle. Table 2 presents these maximum values, and the ratio $N_{\hat{B}_{1,2}}/N_f$, in which N_f is the number of cycles at which failure occurred. From this table, it is clear that when both $\hat{B}_1$ and $\hat{B}_2$ have peaked, on average, 20% of the specimen's life time remains. This indicates that the amplitude of the magnetic stray field might be used to determine the fatigue life time of the specimens.

The observed scatter in the magnetic stray field data could be caused by the influence of the initial magnetic state of the specimen, since the specimens were not demagnetised before the tests started. Therefore, the initial magnetisation was unknown at the start of the experiments. Given that even with this unfavourable initial state, promising results were generated, these tests should be repeated with a more careful magnetic preparation of the specimens. Ultimately, in a better controlled environment, i.e. after demagnetisation, the magnetometer might provide a complementary measurement to conventional techniques to monitor fatigue crack growth in ferromagnetic specimens.

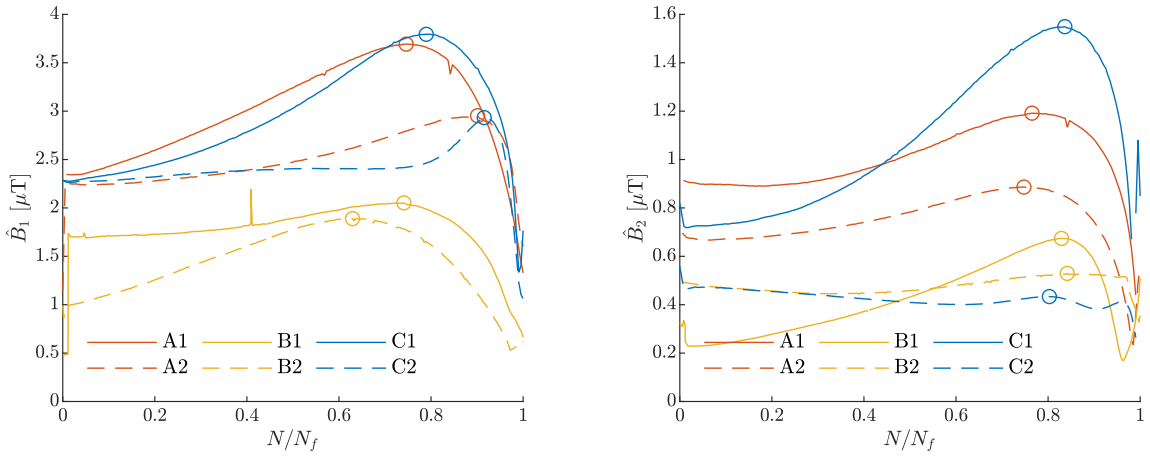

(a) (b)

Figure 7: Amplitude of the (a) first and (b) second principle components of the magnetic stray field with increasing number of cycles. The circle on top of each line indicates the maximum value.

Table 2: Cycle number where the peak in the magnetic stray field amplitude occurred $N_{\hat{B}_1}$ and $N_{\hat{B}_2}$, the cycle number at which the specimen failed N_f, and the ratio of these cycle numbers indicating consumed fatigue life.

Specimen	N_f	$N_{\hat{B}_1}$	$N_{\hat{B}_1}/N_f$	$N_{\hat{B}_2}$	$N_{\hat{B}_2}/N_f$
A1	209 250	156 093	0.75	160 105	0.77
A2	202 625	182 569	0.90	151 476	0.75
B1	170 695	126 487	0.74	141 553	0.83
B2	177 821	111 943	0.63	149 658	0.84
C1	214 584	169 449	0.79	179 479	0.84
C2	213 577	195 525	0.92	171 454	0.80

5. Conclusions

In this study, the experimental results of fatigue tests on CT specimens have been reported. Next to crack gauges, a magnetometer was employed to track the evolution of the magnetic stray field generated by the specimen during crack propagation. The mean value of the time signals of magnetic stray field were determined and the vector components were projected onto their principle axes. From the evolution of the mean value of the stray field, it is clear that three factors influence the measured magnetic response: namely stress, plastic deformation and the displacement of the specimen. Due to the specific stress distribution of the CT specimen, these causes can partially be separated. The large change of the mean value of the stray field indicates that crack initiation can be determined from the magnetic stray field data. Analysis of the RMS amplitude of the magnetic field signals showed that the two dominant components peak before failure of the specimen. At the moment both components peaked, on average, 20% of the specimen's life time remained. By improving the testing conditions, the magnetic field data might provide a complementary measurement for monitoring fatigue crack initiation and growth in ferromagnetic specimens.

Acknowledgments
The authors are grateful to the assistance of Lu Cheng, Georgios Stamoulis, Kees van Beek, Fred Schilperoort and Peter de Vries during the execution of the experiments.

References

[1] Shah M B and Bose M S C 1984 *Physica Status Solidi (a)* **86** 275–281
[2] Vandenbossche L and Dupré L 2009 *Journal of Applied Physics* **105** 07E707
[3] Wang H P, Dong L H, Dong S Y and Xu B S 2014 *Journal of Central South University* **21** 65–70
[4] Zhou W, Fan J, Ni J and Liu S 2019 *Metals* **9** 89
[5] Bao S and Gong S F 2012 *Journal of Applied Physics* **112** 113902
[6] Zhang K, Zhang J, Jin W, Mao J, Li Q and Xu F 2021 *International Journal of Fatigue* **146** 106166
[7] ASTM 2015 Standard Test Method for Measurement of Fatigue Crack Growth Rates Tech. Rep. E647-15 American Society for Testing and Materials
[8] Jolliffe I T and Cadima J 2016 *Philosophical Transactions of the Royal Society A: Mathematical, Physical and Engineering Sciences* **374** 20150202
[9] de Jesus A M, Matos R, Fontoura B F, Rebelo C, Simões da Silva L and Veljkovic M 2012 *Journal of Constructional Steel Research* **79** 140–150
[10] Meijers P C, Jolink C T, Tsouvalas A and Metrikine A V 2022 *International Journal of Mechanical Sciences* **217** 106990